The International Journal of Advanced Manufacturing Technology (2024) 133:3583–3601
https://doi.org/10.1007/s00170-024-13931-y

ORIGINAL ARTICLE

Material removal mechanism of brittle-ductile transition in milling SiC ceramic and experimental verification

Jian Qiu[1,2,3] · **Renpeng Ge**[2] · **Tingchao Han**[2]

Received: 11 December 2023 / Accepted: 26 May 2024 / Published online: 15 June 2024

Abstract

SiC ceramic materials are extremely hard and brittle materials, and are prone to defects such as cracks during processing. It is sensitive to cutting parameters and other processing conditions, making the material extremely difficult to process. This research investigates the material removal mechanism, as well as the influences of cutting parameters and tool wear on the brittle-ductile transition. The relationship between cutting parameters such as feed rate and cutting depth and the ductile–brittle transition was obtained according to the critical load model for brittle material fracture and SiC chip thickness model. Milling tests were conducted, and it was found that with the increase of feed rate and cutting depth, the occurrence of brittle removal increased, and the material removal mode shifted from ductile removal to brittle removal. By the characteristics analysis of force distribution in time–frequency domain, the existence of brittle-ductile transition in SiC milling was proven combined with the analysis of surface roughness and chip morphology. A comprehensive basis for judging the critical transition was provided that the range of parameters is feed rate of 0.015–0.02 mm/z and cutting depth of 0.15–0.2 mm. Tool wear is another significant impact factor on the material removal mode during the milling process. When the tool is worn, it is easier to undergo brittle removal compared to non-worn tools with the same cutting parameters. The brittle-ductile cutting mode of diamond tool milling SiC ceramics and its influence on the cutting force coefficient were also studied based on the milling geometric model. The cutting force mixed with brittle removal and ductile removal is not suitable for identifying the cutting force coefficient.

Keywords SiC ceramics milling · Cutting force coefficient · Brittle–ductile transition · Cutting force · Tool wear

1 Introduction

SiC ceramics is widely used in aerospace, automotive, electronics, optics, and other fields for its advantages of high hardness and good wear resistance. The processing of SiC ceramics can be accomplished by diamond grinding which is the main machining method. Zhou [1] found the critical chip formation thickness and critical ductile–brittle transition thickness based on the mechanic deformation behavior of SiC. Zhang [2] investigated the influence of the dressing method of monolayer brazed diamond wheel on the material removal mechanism. In addition to the traditional grinding methods, SiC ceramics can also be removed by a variety of processing methods. Laser-assisted grinding is a promising method for cost-effective machining of hard and brittle materials, such as (RB)-SiC ceramics [3] and Al2O3 ceramics [4]. Zhang [5] employed an oblique diamond cutting method to improve the brittle−ductile transition behavior of 6H-SiC. Compared to orthogonal cutting, a high compressive stress zone is formed beneath the tool as more materials undergo the squeezing of the elliptic-shaped cutting edge, which is beneficial for promoting the plastic deformation. Sun [6] proposed a ductile machining model for ultra-precision fly cutting to efficiently fabricate deep micro-structures on brittle materials. Ultrasonic vibration was used as an assistant method to solve the ceramics machining problems of high hardness, low efficiency, high cost and easy to break [7].

✉ Jian Qiu
qiuj1981@163.com

[1] College of Engineering, Ocean University of China, Qingdao 266110, China

[2] Shenyang Machine Tool (Group) CO., LTD., State Key Laboratory of High-Grade NC Machine Tools, Shenyang 110020, China

[3] National-Local Joint Engineering Laboratory of NC Machining Equipment and Technology of High-Grade Stone, Shenyang Jianzhu University, Shenyang 110168, China

Zhang [8] analyzed the grinding mechanics and predictive force model based on material-removal and plastic-stacking mechanisms. The influence of lubricating conditions was considered in the force model. Zhao [9] revealed the mechanisms governing machined surface formation of hard brittle monocrystalline 3C-SiC in ultrasonic elliptical vibration-assisted diamond cutting by molecular dynamics simulations, which is useful for decreasing machining force and suppressing crack events. Yang [10] developed a prediction models of minimum chip thickness and ductile–brittle transition chip thickness based on grinding mechanism of friction coefficient in dry grinding, minimum quantity lubrication (MQL) and nanoparticle jet MQL. Chen [11] used different cutting modes as regular cutting, current-feedback cutting, and current-feedback control strategy with high-frequency vibration-assistance to cut Zerodur glass–ceramic based on a semi-ductile cutting depth. He found microcracks created in the cutting process is facilitate to the removal of material, while the negative rake angle of tool inducing press-cut effect is helpful to suppress brittle-fracturing.

The nonconventional machining of ceramics includes ultrasonic machining, abrasive jet machining, abrasive water jet machining, laser machining, electric discharge machining [12]. Laser machining is a good processing method to slice the SiC ceramic. Demarbaix [13] studied on the laser machining with nanosecond source on the ceramic at green stage to determine the influence of input laser parameters. There are also researchers using laser assisted milling to process glass ceramics. Fan [14] in his research developed a glass–ceramic in-situ laser-assisted machining device and found this method can effectively reduce cutting force. The assisting electrode machining is another practical and effective methods to machine SiC ceramics. Researchers like Rao [15] presented research on surface characteristics for RB-SiC ceramics by electrical discharge diamond grinding. Liu [16] carried out a study on SiC ceramics with electrical resistivity of 500 Ωcm by electrical discharge milling to solve the problems of costly and inefficient by using common diamond grinding. Guo [17] studied the influence of the process parameters including polarity of electrode, peak current, pulse-on time and pulse-off time on material removal rate, side gap, and surface roughness. Mohri [18] provide a method with a copper electrode in sinking EDM or with brass wire electrode in WEDM using kerosene as working fluid to machine ceramics, which make the machining very easy. Sánchez [19] described the development of sinking and wire electro-discharge machining technology for ceramics as silicon infiltrated silicon carbide, which could obtain an excellent surface finish and high removal rates for the industrial application.

The hardness and brittleness of ceramics are relative concepts on the macro scale. When the cutting parameters are optimized, the cutting process can be improved to satisfy ductile material removal. The cutting mechanism of brittle-ductile transition has received much attention over the past two decades, especially on the experimental and investigation research. Goel [20] performed an experimental study on diamond turning of single crystal 6H-SiC on an ultra-precision diamond turning machine to elucidate the microscopic origin of ductile-regime machining. They obtained fine surface finish better than any previously reported value on SiC while significant wear marks on the cutting tool was observed. Liang [21] performed an elliptical ultrasonic assisted scratching experiments and found material removal ratio in elliptical ultrasonic assisted grinding of mono crystal sapphire is increased in ductile–brittle transition region. It is prone to achieve ductile region with greater vibration amplitude. Wang [22] presented an investigations of critical cutting speed on ductile-to-brittle transition mechanism by modelling and micrographs observation on chips, chip roots and finished surfaces. Simon [23] described an application of elastic tool combined with rigid pellets and super abrasives to finish aspheric mirror and reduce form error with no residual damage, and studied the mechanics driving brittle-ductile transition on finishing optical ceramic materials. Xiao [24] conducted a molecular dynamics study to investigate the atomic scale details of the cutting zone during the brittle-ductile cutting mode transition.

With the development of diamond cutting tools, the machining of SiC ceramics can also be carried out by diamond milling. Rapid tool wear and high processing cost, poor surface quality control, and low processing efficiency are the difficulties. The most important problem is that the hard and brittle property of ceramics is easy to produce cracks in the cutting process. In this paper, the cutting mechanism of SiC ceramics using diamond tool on a machining center was analyzed, and the analysis of brittle-ductile transition of SiC was presented. Attention was paid to the comprehensive judgment of brittle-ductile transition of SiC milling by force signal, surface quality, and chip forms. Tool wear and cutting parameters are focused on for the transition of material removal mode and force characteristics in the milling process. The purpose of this research is to master the critical parameter interval of brittle-ductile transition, and to optimize cutting parameters, to achieve high efficiency and high quality.

1.1 Analysis of brittle-ductile transition of milling

1.1.1 Chip formation analysis based on stress–strain

The chip formation of cutting is simplified in Fig. 1. Materials in the tool tip is under the action of the compression stress. Due to the different movement directions of the chip and the machined surface, the chip separation area I that contacts with the tool's rake face mainly bears

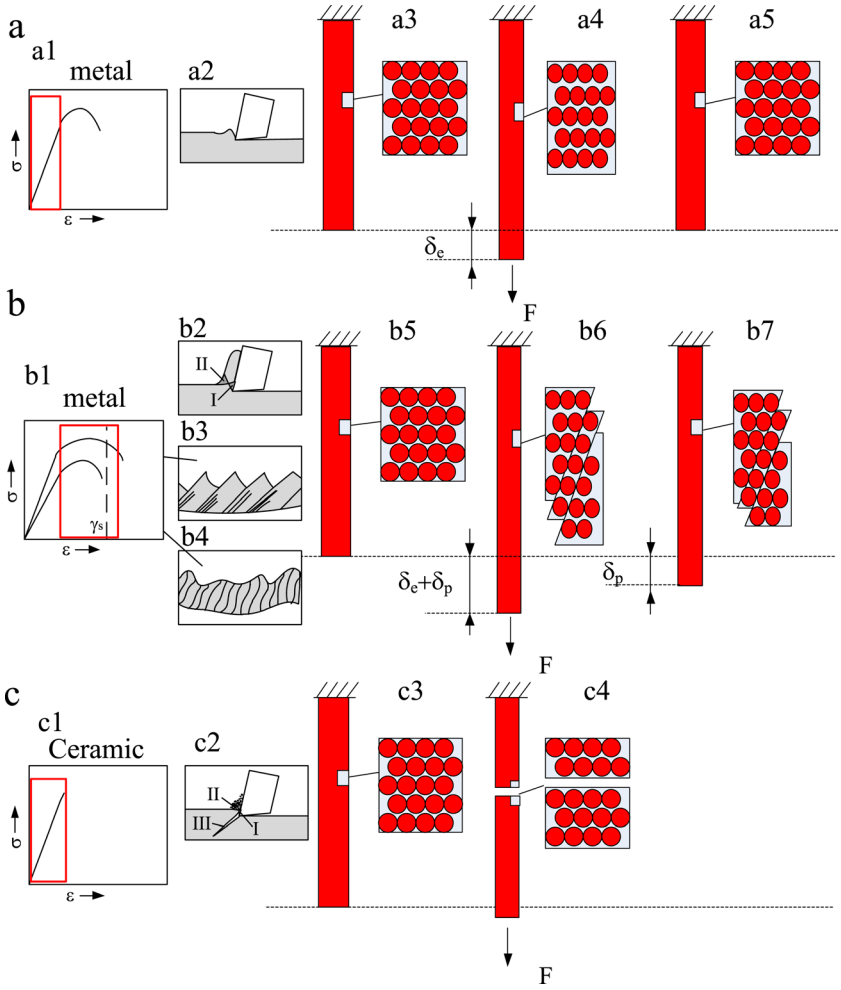

Fig. 1 Chip formation mechanisms and stress-stain comparison of metal and ceramics. (a. elastic deformation of metal. b. ductile deformation of metal. c. brittle deformation of ceramics. F is force, δ_e and δ_p are the elastic deformation and ductile deformation)

tensile stress from material removal, while the second main stress area II is mainly subjected to the compressive stress produced by chip bending, as shown in Fig. 1a and Fig. 1b. If the tensile force does not reach the material yield strength, the metal material is deformed by the loading force F (Fig. 1a4) in the elastic deformation stage as shown in stress–strain curve of Fig. 1a1. When the force F is unloaded, the material rebounds almost without deformation (Fig. 1a5). The chips slip along the tool's rake face, and break apart after curling to fracture strength. The morphology of chips is related to material properties and cutting parameters. Sawtooth chips (Fig. 1b3) and curling chips (Fig. 1b4) can be formed under different conditions. When the tensile force exceeds the yield strength of the material, permanent deformation occurs, as shown in Fig. 1b. In the stage of ductile deformation in Fig. 1b1, the material deforms under the action of force F (Fig. 1b6). When the force is unloaded, the material is partly rebound, but the overall deformation is larger than before loading (Fig. 1b7). The geometric of metal will change before fracture, and some phenomena can be used to predict fracture.

If the material is brittle, the ceramics will hardly deform before break, as shown in Fig. 1c. From the stress–strain curve of ceramics material, it is approximately consistent with Hooke's law when the stress produced by the loading force is small, as shown in Fig. 1c1, and the material will not yield as there is no yield stage in the curve. When the loading force is beyond the critical force, material broken almost with no ductile deformation but break (Fig. 1c4), the sawtooth chips are prone to fracture and form powder chips.The transition of ceramics from ductile cutting to brittle cutting can be explained as: When the cutting thickness does not exceed the critical value of brittle-ductile transition, the material cutting mode are mainly ductile removal. The deformation of ceramics materials in the tool tip is similar to metal. The brittle material is forced under the action of the compression stress in the separation area I and the second main stress area II in Fig. 1c2. Subsequently, the ceramics materials at the tool tip fracture, and the chips separate from workpiece along the rake surface of cutting tool. With the continuous increasing of stress in region I and region II, the chips are gradually stripped from the ceramics workpiece

gradually. And the separated chips are broken into powder chips under the influence of extrusion stress in region II. The existence of ceramic chips is probabilistic, and the Webb distribution function can be used to describe the fracture of a chip, as shown in Eq. (1).

$$f_c(\sigma) = 1 - \exp[-(\frac{\sigma}{\sigma_0})^m \int_v (\frac{\sigma\prime}{\sigma})^m dv] \quad (1)$$

where, $f(\sigma)$ is fracture probability; m is Webb coefficient, the greater the value, the smaller the probability of fracture; σ_0 is characteristic stress; σ and σ' are the internal stress and its maximum value.

The critical load P required for the crack initiation of ceramics with respect to the toughness and hardness of the ceramics material is given in Eq. (2), and the crack length l of ceramics cutting is present in Eq. (3) [21].

$$P = \lambda_0 \frac{K_c^4}{H^3} \quad (2)$$

$$l = \mu_0 \frac{K_c^2}{H^2} \quad (3)$$

where, λ_0 and μ_0 are geometric constants related to materials properties; P is critical load, kPa; l is crack length, μm; K_c is fracture toughness, which is a characterization to resistance material fracture; H is material's hardness.

The critical chip thickness of ceramics cutting can be extended from the critical indentation size in the indentation fracture mechanics [25] as shown in Eq. (4).

$$h_{CIS} = K\frac{E}{H}(\frac{K_c}{H})^2 \quad (4)$$

where, E is elastic modulus, GPa, K is the coefficient relate to critical chip thickness.

When the cutting thickness beyond the critical value of brittle-ductile transition, cutting of brittle materials produces significant volume expansion before broken and chip formation. The strain produced by ceramic cutting under steady load tends to be inelastic and non-recoverable as Fig. 1c1 shows. It is difficult to describe the chip shape in the deformation of ceramic cutting. The chip geometric of ceramics is different from the undeformed chip with no broken calculated in Eq. (1). The undeformed chip will crack under the deformation force as shown in Fig. 1c2. These cracks tend to expand, causing chips to break suddenly in a very small form and further to fracture. Therefore, the cutting of ceramics will cause chips to break, and the broken chip will form powder like particles.

When the cutting thickness beyond the critical value, it generates crack in the process of chip separation, the cracks on the interface of chip-workpiece in the stress region I are tensile stress crack, and the cracks produced on the machined surface in the stress region II are compressive stress cracks. The tensile stress cracks have great influence on the machined surface for their special position, while the compressive stress cracks tend to crush the ceramics material. The appearance of cracks will accelerate the process of material removal, and the material removal mode will change from ductile to brittle. Cracks will extend to the machined surface easily to form machined surface defects, as shown in Fig. 1c2 III. The cutting process of ceramics is a combination of ductile removal and material removed with micro fracture. Tool geometry and cutting parameters have influence on the morphology of ceramics removal. The absolute ductile deformation occurs only in the processing condition [26] below the critical values.

1.1.2 Critical stability interval of brittle-ductile transition

Lawn and Marshall [25] proposed an empirical relationship model between the critical load and the crack length on the machined surface. The ductile material removal model of SiC ceramics milling with straight diamond tool can be seen as shown in Fig. 2. In Fig. 2a, when the chip thickness h reaches a critical thickness of h_c, the material begins to be removed from ductile to brittle. If the chip thickness is less than the critical thickness, material removal mode can be considered as ductile removal. Conversely, initial cracks will generate. When the cracks generate, it will extend to the ceramics surface and result in

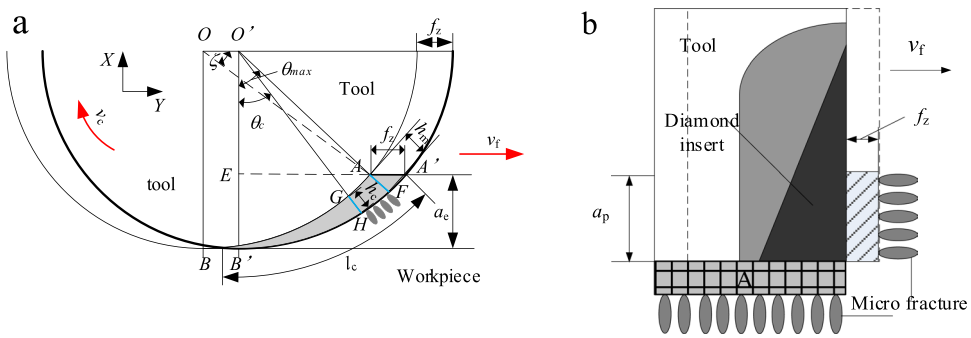

Fig. 2 Milling geometry model. (a. top view; b. side view)

processing defective, it tends to brittle removal. In Fig. 2b, a critical chip thickness region in the depth direction of the milling cutter exists as shown in the *A* region. In the case of small cutting depth, the brittle fracture will not be directly excited, and it will be in a stable cutting state.

The critical undeformed chip thickness and chip length in the milling process can be seen in Eq. (5)[27, 28].

$$\begin{cases} h_c = f_z\sqrt{\frac{2a_e}{R} - \frac{f_z^2}{2R}} = f_z sin\theta_c \\ l_c \approx \sqrt{2a_e R} \end{cases} \tag{5}$$

where, h_c is the critical undeformed chip thickness, mm; f_z is the feed rate per tooth, mm/z; a_e is the cutting width, mm; R is the radius, mm; l_c is the chip length, mm; The angle corresponding to the maximum undeformed chip thickness θ_c=arccos($\frac{R-a_e}{R-h_c}$).

When the undeformed chip thickness h is equal to the critical thickness h_c, the critical feed rate per tooth can be obtained, as shown in Eq. (6).

$$f_{zc} \approx h_c\sqrt{\frac{R}{2a_e}} \tag{6}$$

The conditions to achieve the ductile cutting of SiC ceramics [29, 30] for ideal surface are $h \le h_c$.

When cutting width is full width, the cutting width a_e of the model in Fig. 2 is equivalent to the tool radius R. Currently, the contact length between the tool and the workpiece is $\pi R/2$. The angle θ_c is $\pi/2$. As a result, the undeformed chip thickness is feed rate per tooth of tool, $h=f_z$. The critical conditions is $f_z \le h_c$.

Table 1 Specifications of machine tool

Index	Specifications
Maximum stroke of worktable—X-axis, mm	850
Maximum stroke of sliding seat—Y axis, mm	500
Maximum stroke of spindle—Z axis, mm	540
Revolution range, r/min	50 ~ 8000
Feed speed, mm/min	1–10,000
Positioning accuracy X / Y / Z, mm	0.020/0.015/0.015
Repeat positioning accuracy X / Y / Z, mm	0.012/0.010/0.010

2 Experiments

2.1 Experimental set-up

The cutting test was carried out on a NC machining center VMC850e manufactured by Shenyang Machine Tool Group. The specifications of milling machine are shown in Table 1. The test equipment is shown in Fig. 3. The diamond milling tool was used for cutting slot cutting of SiC ceramics. And the cutting force was recorded by a six-component force dynamometer of Kistler 9265B, Kistler 5070 charge amplifier, and Dynoware software. A microscope of Keyence VHX2000 was used to test tool wear, machining surface and chips, while a 3D profiler was used to measure the surface roughness. The new tool is shown in Fig. 3def.

2.2 Test workpiece and cutting tool

In the cutting test, the workpiece is SiC ceramic with size of 120 mm × 80 mm × 80 mm. The material properties

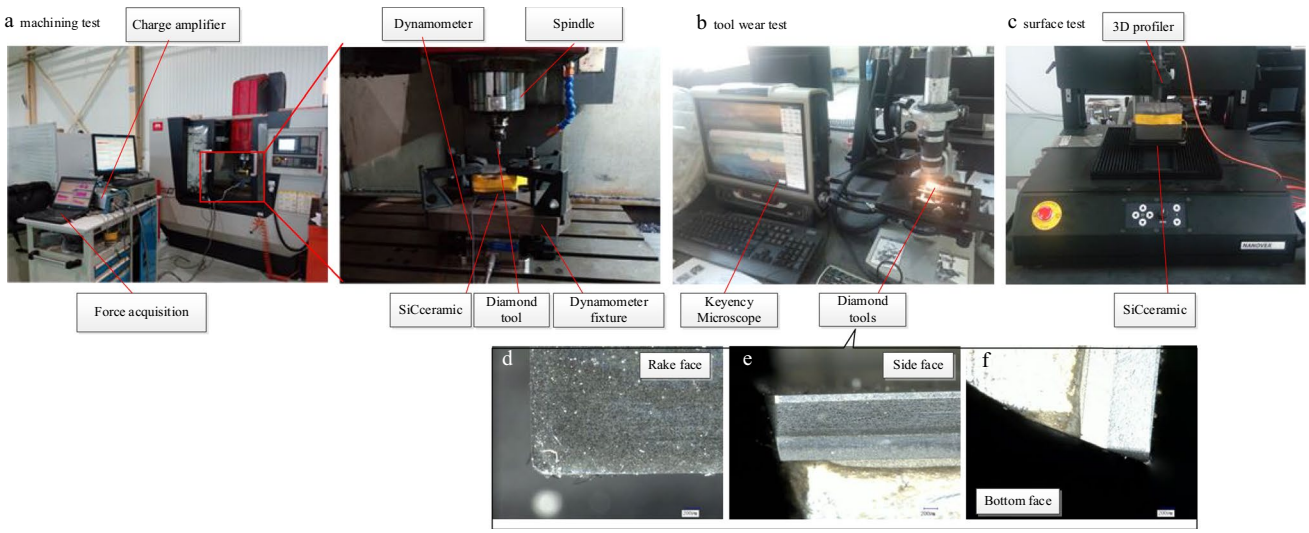

Fig. 3 Tests of SiC ceramics milling (a. machining test; b. tool wear test; c. surface tests; def. rake, side, and bottom faces of new tool)

of SiC ceramics and characteristics of diamond tool are shown in Table 2. The workpiece was clamped tightly in jaw vice.

2.3 Cutting test design

Single factor experiments were designed to test the cutting parameters region of brittle-ductile transition regarding the influences of cutting parameters. The cutting test was designed for tool full width milling. Exp.I was designed for single factor test of variable spindle speed corresponding to different cutting depths and single factor of variable feed rate. Exp.II using similar parameters with Exp.I was set for duplicate validation. Exp.III was designed for the effect of feed rate for different parameters range. All the cutting parameters are shown in Table 3.

3 Results and discussion

3.1 Cutting force distribution of brittle materials in ductile removal mode

3.1.1 Cutting force distribution

The cutting force distribution results in the variable cutting depth experiment are shown in Fig. 4a. The cutting parameters are $n = 1000$ r/min, $a_p = 0.05, 0.1, 0.15, 0.2$ mm, $f_z = 0.01$ mm/z. The cutting forces in the three directions also increase with the increase of material removal amount. The cutting force in the Z direction is most severely affected by cutting parameters. From the trend of cutting force changes, no significant brittle removal was found, indicating that the cutting with these cutting parameters is ductile removal mode. According to the principle shown in Fig. 1, the cutting depth has a small impact on the quality of ceramic processing.

The results of the variable spindle speed test are shown in Fig. 4b. The cutting parameters: $a_p = 0.15$, $f_z = 0.01$ mm/r, $n = 1000$, 2000, 3000, 4000 r/min, and the corresponding material removal rates are $MRR = 48$, 96, 144, 192 cm^3/min. The cutting forces in all three directions increase with the increase of spindle speed. As the spindle speed increases, when the tool diameter is fixed, the cutting speed correspondingly increases, and the ceramic material located in the cutting zone softens due to the increase in temperature. The toughness of the material is improved, the yield strength is reduced, and the cutting mode shifts from brittle fracture to ductile removal. In addition, as the cutting speed increases, the strain rate of the material increases, the material removal rate increases, and thus the cutting force increases. However, the occurrence of the above phenomenon is not obvious.

In addition, based on the Salomon curve in high-speed machining, it can be predicted that there is an optimal range of cutting speed for SiC ceramics. When this range is exceeded, the impact of cutting temperature and wear will cause a sharp decrease in tool life. Based on the previous analysis of cutting surface cracks and surface roughness, under the same conditions, the higher the spindle speed, the more significant the residual cracks on the machining surface. In the cutting process of SiC ceramics, the influence of cutting speed on machining quality and tool life is most prominent [9, 20].

The distribution of cutting force corresponding to the variable feed cutting test is shown in Fig. 4c, where $n = 3000$ r/min, $a_p = 0.1$ mm, $f_z = 0.005, 0.01, 0.015, 0.02$ mm/z. The cutting force distribution is like that in the variable cutting depth test. The forces increase linearly with feed rate increasing when the tool is not worn.

3.1.2 The time–frequency domain characteristics of cutting force with no wear tool

Taking the variable feed rate cutting test as an example, the time–frequency characteristics of cutting force can be analyzed. When the feed rate increases from 0.005 to 0.015 mm/z, the numerical envelope of cutting force in the time domain increases with the increase of feed rate. The force peak in frequency domain also slightly increases, and the frequency of cutting force is mainly the tooth frequency caused by tool rotation. A frequency peak appears near 700 Hz, indicating that ductile removal has chatter components, and ductile removal is the main removal mode. Both ductile and brittle removal exist simultaneously. When the feed rate continues to increase

Table 2 Material properties and tool parameters [29]

Material characteristics	Value
Fracture toughness K_c, MPa $m^{1/2}$	1.9
Hardness H, GPa	22
Elastic modulus E, GPa	347.01
Critical crack length Y_c, μm	0.895
Critical chip thickness h_{cis}, μm	0.01764
Tool characteristics	Value
tool manufacturer	Self-made
Material	Diamond tool
Tool angle	90°
Cutting edge angle	90°
Tool diameter	16
Tooth number	2
Inclined angle	0°
Edge shape	Straight

Table 3 List of cutting parameters

Exp.I—effect of spindle speed and cutting depth and feed rate (VMC850e)						
n, r/min	Δn, r/min	f_z, mm/z	Δf_z, mm/z	a_p, mm	Δa_p, mm	MRR, cm^3/min
1000	-	0.01	-	0.1	-	32
2000	1000	0.01	-	0.1	-	64
3000	1000	0.01	-	0.1	-	96
4000	1000	0.01	-	0.1	-	128
1000	-	0.01	-	0.2	-	64
2000	1000	0.01	-	0.2	-	128
3000	1000	0.01	-	0.2	-	192
4000	1000	0.01	-	0.2	-	256
1000	-	0.01	-	0.15	-	48
2000	1000	0.01	-	0.15	-	96
3000	1000	0.01	-	0.15	-	144
4000	1000	0.01	-	0.15	-	192
3000	-	0.005	-	0.1	-	48
3000	-	0.01	0.005	0.1	-	96
3000	-	0.015	0.005	0.1	-	144
3000	-	0.02	0.005	0.1	-	192
2000	-	0.01	-	0.1	-	64
3000	1000	0.01	-	0.1	-	96
4000	1000	0.01	-	0.1	-	128
2000	-	0.01	-	0.2	-	96
3000	1000	0.01	-	0.2	-	176
4000	1000	0.01	-	0.2	-	256
Exp.II—effect of single cutting parameter (VMC850e)						
1000	-	0.01	-	0.15	-	48
2000	1000	0.01	-	0.15	-	96
3000	1000	0.01	-	0.15	-	144
4000	1000	0.01	-	0.15	-	192
3000	-	0.005	-	0.1	-	48
3000	-	0.01	0.005	0.1	-	96
3000	-	0.015	0.005	0.1	-	144
3000	-	0.02	0.005	0.1	-	192
1000	-	0.01	-	0.05	-	16
1000	-	0.01	-	0.1	0.05	32
1000	-	0.01	-	0.15	0.05	48
1000	-	0.01	-	0.2	0.05	64
Exp.III—effect of feed (VMC850e)						
2000	-	0.005	-	0.1	-	40
2000	-	0.01	0.005	0.1	-	80
2000	-	0.015	0.005	0.1	-	120
2000	-	0.02	0.005	0.1	-	160
2000	-	0.025	0.005	0.1	-	200

*Δn, Δf_z and Δa_p are the increasing steps of spindle speed, feed rate, and cutting depth

to 0.02 mm/z, the force envelope in the time domain decreases. The peak value of high-frequency components in the frequency domain decreases, indicating that material removal has shifted from ductile removal to brittle removal, and both ductile and brittle removal still exist simultaneously (Fig. 5).

3.1.3 Cutting force characteristics under ductile removal mode

By analyzing the combination of cutting forces in X and Y directions in the whole cutting process, the characteristics of cutting force within the time history under ductile removal

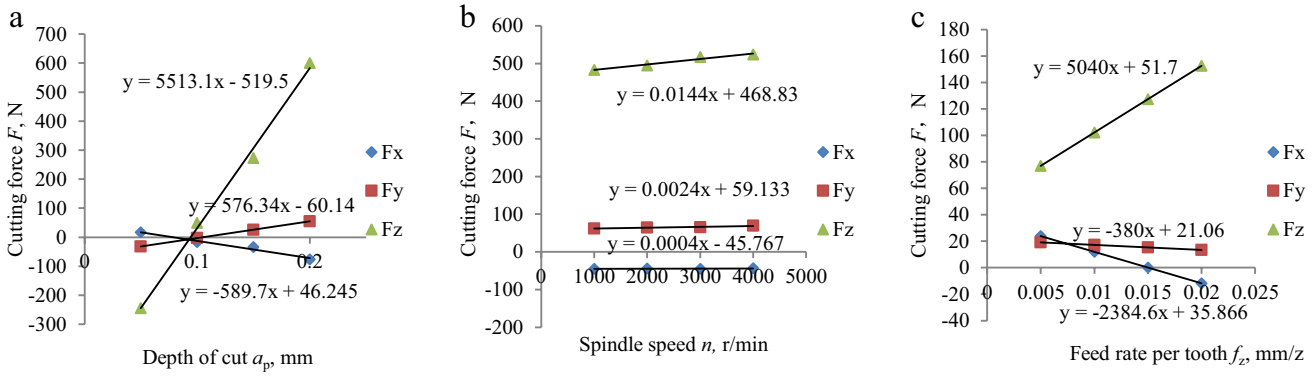

Fig. 4 The distribution of cutting forces with cutting parameters. (a. variable cutting depth test; b. variable spindle speed test; c. variable feed rate test, second workpiece, tool worn)

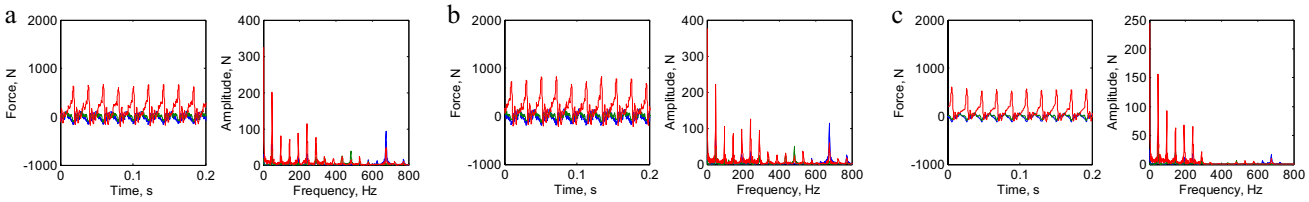

Fig. 5 The time–frequency domain characteristics of cutting force in the variable feed rate test. (a. $f_z = 0.005$ mm/z, $n = 3000$ r/min, $a_p = 0.1$ mm; b. $f_z = 0.015$ mm/z, $n = 3000$ r/min, $a_p = 0.1$ mm; c. $f_z = 0.02$ mm/z, $n = 3000$ r/min, $a_p = 0.1$ mm)

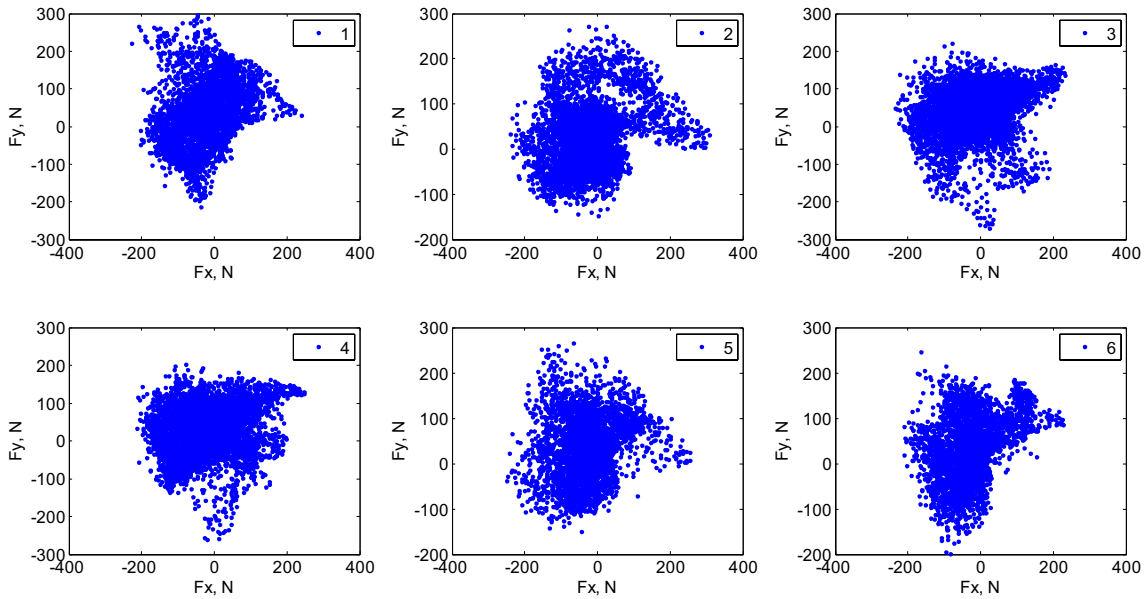

Fig. 6 X–Y plot of cutting forces. (a. 1/6 of the total time; b. 1/3 of the total time; c. 1/2 of the total time; d. 2/3 of the total time; e. 5/6 of the total time; f. 1 of the total time)

mode could be analyzed. The cutting parameters are $n = 4000$ r/min, $f_z = 0.01$ mm/z, $a_p = 0.1$ mm. From Fig. 6, it can be found that the X–Y plot of cutting forces is variable with cutting time. The range of forces trajectory at the early cutting stage is large and discrete. In the later stage of cutting process, the range of the trajectory in the Y axis is larger while the X axis is smaller.

3.2 Influence of tool wear on the distribution of cutting force

3.2.1 The effect of tool wear on material removal mode

Figure 7 shows the distribution of cutting force with the same cutting parameters in the variable feed cutting test when the tool is worn. Compare the mean cutting force of two test at the same parameters with the tool in different wear condition as shown in Fig. 4c and Fig. 7. Due to tool wear during the cutting of the second test, the cutting forces during the first two cutting parameters of $f_z = 0.005$ mm/z and $f_z = 0.01$ mm/z are greater than those of the first test. However, when the cutting force reaches the critical value of material fragmentation, such as 0.015 mm/z, the cutting force begins to decrease, and as the cutting feed continues to increase, the cutting force decreases significantly, indicating a change in the material removal mode and a shift towards brittle removal as the main method of cutting. As the feed parameter continues to increase, the cutting force of the worn tool shows a decreasing trend. By parameter 0.02 mm/z, it has been shown that the cutting force of the worn tool is smaller than that of the unworn tool, further proving that tool wear leads to a change in material removal mode from ductile removal to brittle removal.

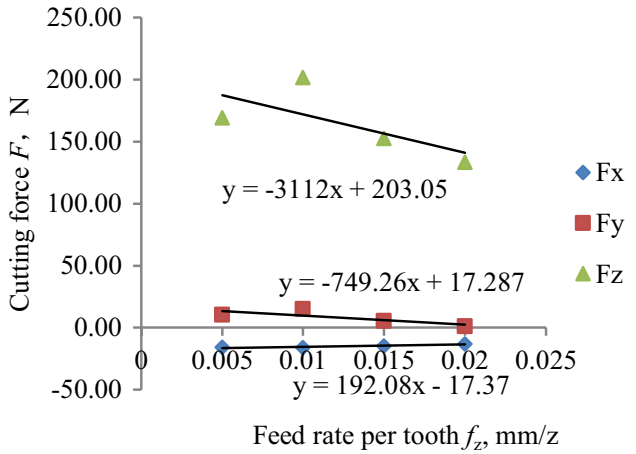

Fig. 7 Same parameter variable feed cutting force. (first workpiece, Tool not worn)

Figure 8 shows the mean cutting forces comparisons before and after tool wear in the variable feed rate cutting when $n = 3000$ r/min, $a_p = 0.1$ mm. It is found that the cutting forces F_x and F_y with worn tool are larger than that of unworn tool as the cutting edge are worn into arc and the forces in X and Y direction are distributed to the radial direction of the tool. And the cutting modes before and after tool wear are different. For the worn tool, cutting mode is brittle when the feed rate per tooth exceeds 0.015 mm/z and the cutting forces decrease significantly. The change in material removal mode will affect the identification results of cutting force coefficient.

3.2.2 Data consistency on the transition of ductile–brittle removal

Taking the test of changing the speed and cutting depth after tool wear as an example to illustrate the consistency of the test data. Figure 9 shows the distribution of cutting force with cutting depth in the variable cutting depth test at spindle speeds of 2000 r/min, 3000 r/min, 4000 r/min, and feed rate of 0.01 mm/z. The distribution of data is almost consistent, with a decrease in cutting force when the cutting depth reaches 0.15 mm or above. This

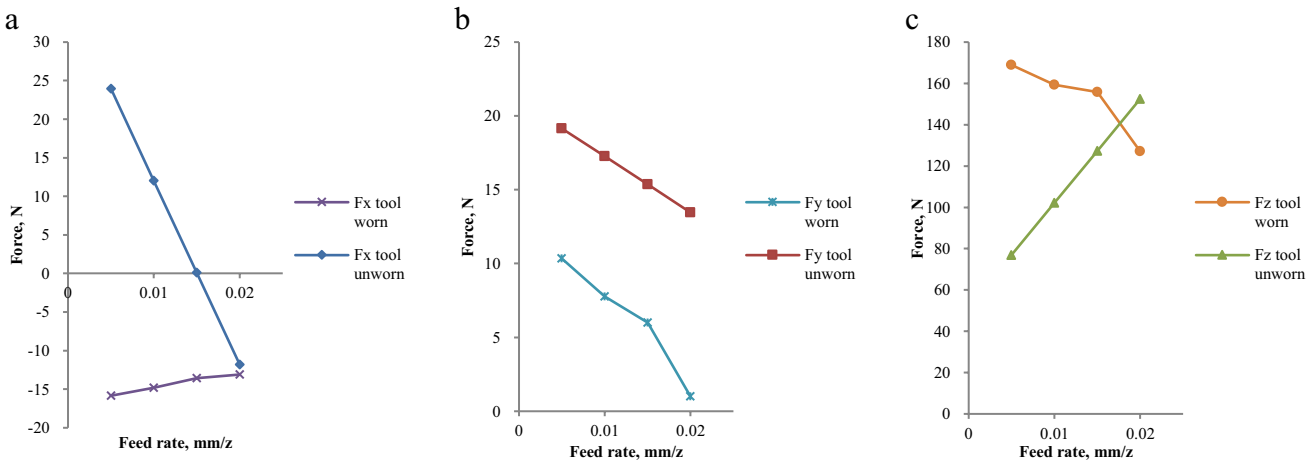

Fig. 8 Cutting forces distribution in variable feed milling with the same parameter before and after tool wear

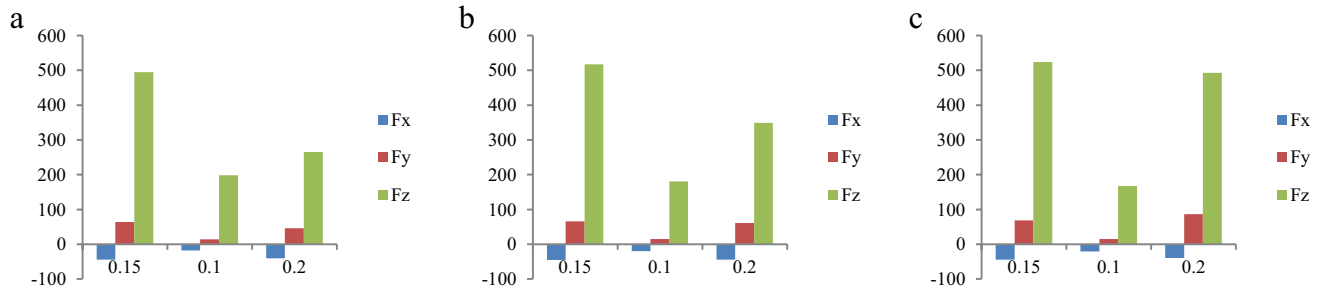

Fig. 9 Cutting force distribution after tool worn. (a. $n = 2000$ r/min; b. $n = 3000$ r/min; c. $n = 4000$ r/min)

trend is inconsistent with the trend of increasing cutting force with increasing cutting depth in ductile cutting, such as metal cutting, indicating that brittle removal occurs above this cutting parameter. From the comparison of cutting forces at spindle speed of 2000 r/min, 3000 r/min, and 4000 r/min, it can be found that the change of material removal mode from ductile removal to brittle removal during the change in cutting depth from 0.15 to 0.2 mm does not due to the change in spindle speed. All these changes occurred during the transition from ductile removal to brittle removal during the cutting depth from 0.15 to 0.2 mm.

4 Identification of SiC ceramic milling force coefficients in ductile mode and brittle mode

The milling cutting force coefficient can be used to fit the linear slope and intercept in the X, Y, and Z axes of the machine tool using the mean cutting force, and calculated as shown in Eq. (7) and Eq. (8).

$$\begin{bmatrix} \overline{F}_x \\ \overline{F}_y \\ \overline{F}_z \end{bmatrix} = \begin{bmatrix} -\frac{K_{nc}}{4} \\ \frac{K_{tc}}{4} \\ \frac{K_{ac}}{\pi} \end{bmatrix} Na_p f_z + \begin{bmatrix} -\frac{K_{ne}}{\pi} \\ \frac{K_{te}}{\pi} \\ \frac{K_{ae}}{2} \end{bmatrix} Na_p \tag{7}$$

where, N is the number of tool tooth; K_{nc}, K_{tc}, K_{ac} are the cutting force coefficients in normal, tangential, and axial directions; K_{ne}, K_{te}, K_{ae} are the edge force coefficients in normal, tangential, and axial directions; f_z is the feed rate per tooth, mm/z; a_p is the depth of cut, mm.

$$\begin{aligned} K_{tc} &= \frac{4\overline{F}_{yc}}{Na_p}, K_{te} = \frac{\pi\overline{F}_{ye}}{Na_p} \\ K_{nc} &= \frac{-4\overline{F}_{xc}}{Na_p}, K_{ne} = \frac{-\pi\overline{F}_{xe}}{Na_p} \\ K_{ac} &= \frac{\pi\overline{F}_{zc}}{Na_p}, K_{ae} = \frac{2\overline{F}_{ze}}{Na_p} \end{aligned} \tag{8}$$

where, $\overline{F}_{xc}, \overline{F}_{yc}, \overline{F}_{zc}, \overline{F}_{xe}, \overline{F}_{ye}, \overline{F}_{ze}$ are the slopes and intercepts of the fitted lines of the mean cutting force along the three axes with respect to the feed rate.

When identifying the cutting force coefficient of SiC ceramic materials during milling processing, due to the different modes of the material removal, and even the same brittle removal with different degrees of fragmentation, there are high requirements for identifying whether the cutting force coefficient is meaningful as it is affected by the accuracy of the identification results. The ceramic cutting force coefficients obtained within the ductile removal range when the tool is not worn are shown as the first row in Table 4. The cutting force coefficient of SiC ceramics given at this time was obtained when the diamond milling cutter is not worn, and no obvious brittle removal was observed.

4.1 Transition of ductile–brittle removal mode

4.1.1 Transition of ductile–brittle removal mode with cutting parameters

The relationship between cutting parameters such as feed rate and radial depth of cut and ductile—brittle transition is concluded in Fig. 10. The critical value a_{pc} and f_{zc} are the critical axial depth of cut and the critical feed rate.

a. When the feed rate and depth of cut are much smaller than the critical value, the interaction between abrasive

Table 4 SiC cutting force coefficient with brittle removal mode

Tool condition	K_{xc}	K_{yc}	K_{zc}	K_{xe}	K_{ye}	K_{ze}
Unworn	-23,846	-3800	50,400	358.66	210.6	517
Worn	1914.3	-5958.5	25,828	-167.36	137.26	1850.7

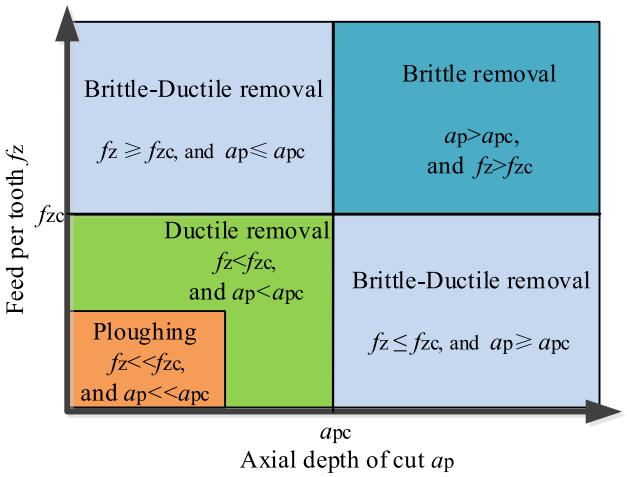

Fig. 10 Critical condition of brittle-ductile cutting transition

grain and workpiece is ploughing. The material mainly undergoes ductile deformation and is hardly removed.

b. When the feed rate and depth of cut are smaller than the critical value but not so much smaller, the material are mainly removed as ductile removal.
c. When the depth of cut is larger than the critical value and the feed rate is smaller than the critical value, the cutting cracks will generate. The material is removed as brittle removal accompanied by ductile removal.
d. When the feed rate is larger than the critical feed rate and the depth of cut is smaller than the critical depth of cut. The mechanism of crack formation during ceramics cutting is the same as that of indentation fracture mechanics. The material removal is brittle—ductile removal.

c and d. When any parameter of depth of cut or feed rate is greater than the critical value, the material removal includes brittle thickness and ductile thickness. The fracture of ceramics materials is a combination of material properties and external loads, and undeformed chip morphology. The material will be removed as brittle mode, accompanied by ductile mode.

e. When the feed rate and cutting depth satisfy both of the parameters are smaller than the critical value, brittle removal generates. In addition,

The ceramics cutting generally have different degrees of micro cracks appear [31, 32]. The fracture strength of brittle materials does not depend on the number of microcracks, but depends on the length and depth of microcracks.

Table 5 Tendency of material removal mode transition with cutting parameters increasing

Parameter increase	Strain hardening	Strain softening	Material removal mode transition
Spindle speed from 1000 to 4000	↑	↓	ductile → brittle
Cutting depth from 0.05 to 0.2	↑	↓	ductile → brittle
Feed rate from 0.005 to 0.02	↑	↓	ductile → brittle

When the crack size exceeds a certain value, it will expand rapidly.

Table 5 shows the tendency of material removal mode transition with cutting parameters increasing according to the experimental data. With the increasing of spindle speed, cutting depth and feed rate, the effect of material strain hardening increases and strain softening decreases. As a result, the material removal mode changes from ductile to brittle.

4.1.2 Other supporting evidence to prove the change of material removal mode

(1) Comparison of chip morphology

Figure 11 shows the comparison of chip form between brittle milling and ductile milling. The parameters of brittle removal are $n = 1000$ r/min, $f_z = 0.01$ mm/z, $a_p = 0.2$ mm, while the parameters of ductile removal are of $n = 3000$ r/min, $f_z = 0.015$ mm/z, $a_p = 0.1$ mm. Evidence shows that the region *B* of brittle removal in Fig. 11ab has a lot of tiny cracks on the machined surface. The crack propagation in the cutting process is very easy to cause massive spalling due to the low bonding strength of SiC ceramics, especially at the shoulder of cutting groove, as region *A* shown in Fig. 11a. The chips produced at the two sides of the groove shoulders are block chips formed by brittle fracture as shown in Fig. 11c.

When the cutting depth decreases and relative larger spindle speed and feed rate, the machined surface shows no obvious micro cracking, such as region *C* of ductile removal in Fig. 11d and Fig. 11e. Currently, both sides of the groove shoulders are integrity and no material spalling (Fig. 11d). The chips are powder chips with the same morphology as Fig. 11f shows.

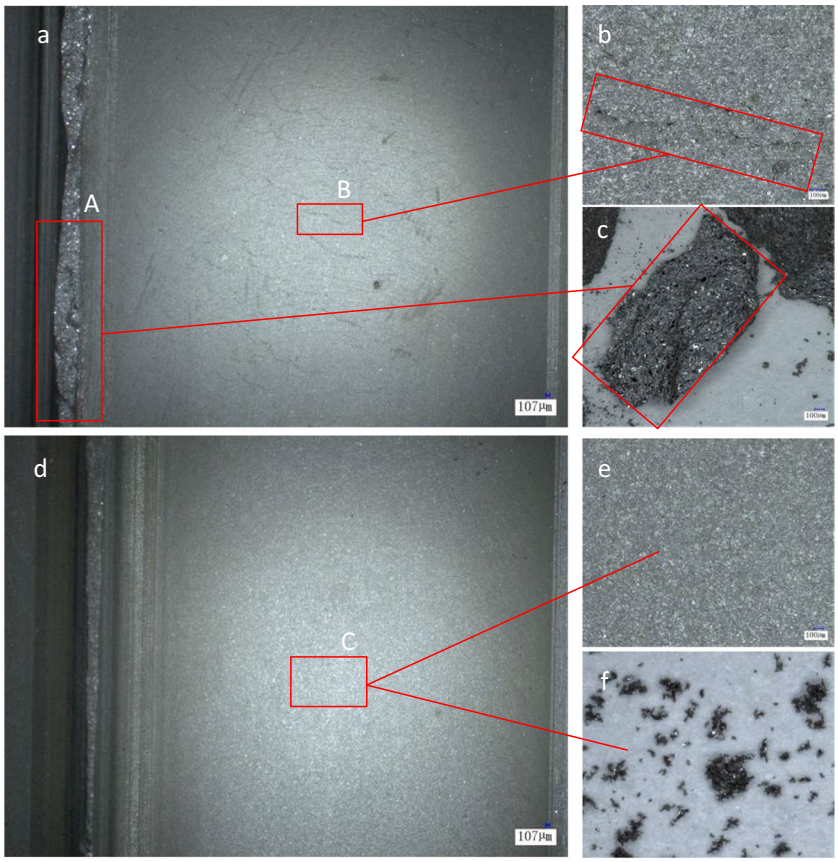

Fig. 11 Surface integrity. (a, b. poor quality surface with material spalling induced by crack, $n=1000$ r/min, $f_z=0.01$ mm/z, $a_p=0.2$ mm; c. block chip from poor quality surface; d, e. high quality surface, $n=3000$ r/min, $f_z=0.015$ mm/z, $a_p=0.1$ mm; f. powder chip from high quality surface)

(2) Surface counter and roughness

Surfaces were compared to determine the effect of cutting parameters on the brittle-ductile transition [33]. Some researchers used 3D profilometer [34] or SEM [35] to study the brittle–ductile transition of brittle materials cutting. When the cutting parameters especially feed rate decreases, an increase in ductile removal proportion is presented. In the variable feed rate cutting test, the surface roughness and the skewness coefficient increase linearly with the feed rate increases from 0.005 to 0.015 mm/z, while the kurtosis coefficient decreases linearly. When the feed rate reaches 0.02 mm/z from 0.015 mm/z, the tendencies of the surface roughness indexes of S_q and S_a (Fig. 12a), S_{sk} and S_{ku} (Fig. 12b) change to the opposite position.

The cutting mechanism of SiC ceramics is different from ductile shear in metal cutting, but also different from the usual brittle fracture in high brittle material removal. Brittle fracture accompanies with ductile deformation in the milling process of ceramics, and the proportion of the two kinds of material removal mode is uncertain with the different processing conditions and material properties.

Evidence in Table 6 shows that the material removal mode changes from ductile removal to brittle removal in this interval of cutting depth from 0.15 to 0.2 mm and feed rate from 0.015 to 0.02 mm/z. The critical interval of cutting depth is affected by tool wear as the worn tool at small cutting depth will lead to material breakage, which makes the material removal mode transition. The evidence of micro surface in Table 6 shows that cracks occur when the depth of cut is less than 0.1 mm. This phenomenon is not due to the brittle-ductile transition of hard and brittle materials, but rather because the cutting tool plows the brittle material and presses out cracks when the depth of cut is less than the radius of the tool radius.

From the two-dimensional contour of Fig. 12c1–c3, the milling marks of the cutter can be seen on the surface in the feed rate range of 0.005–0.015 mm/z, especially at feed rate of 0.015 mm/z (Fig. 12c2). However, when the feed rate increases to 0.02 mm/z, as shown in Fig. 12c3, the milling marks disappear. Based on the contour surface pores in Fig. 12d1–d3, it can be found that at feed rate of 0.02 mm/z, as shown in Fig. 12d3, a large number of pore defects appear on the surface, and crack

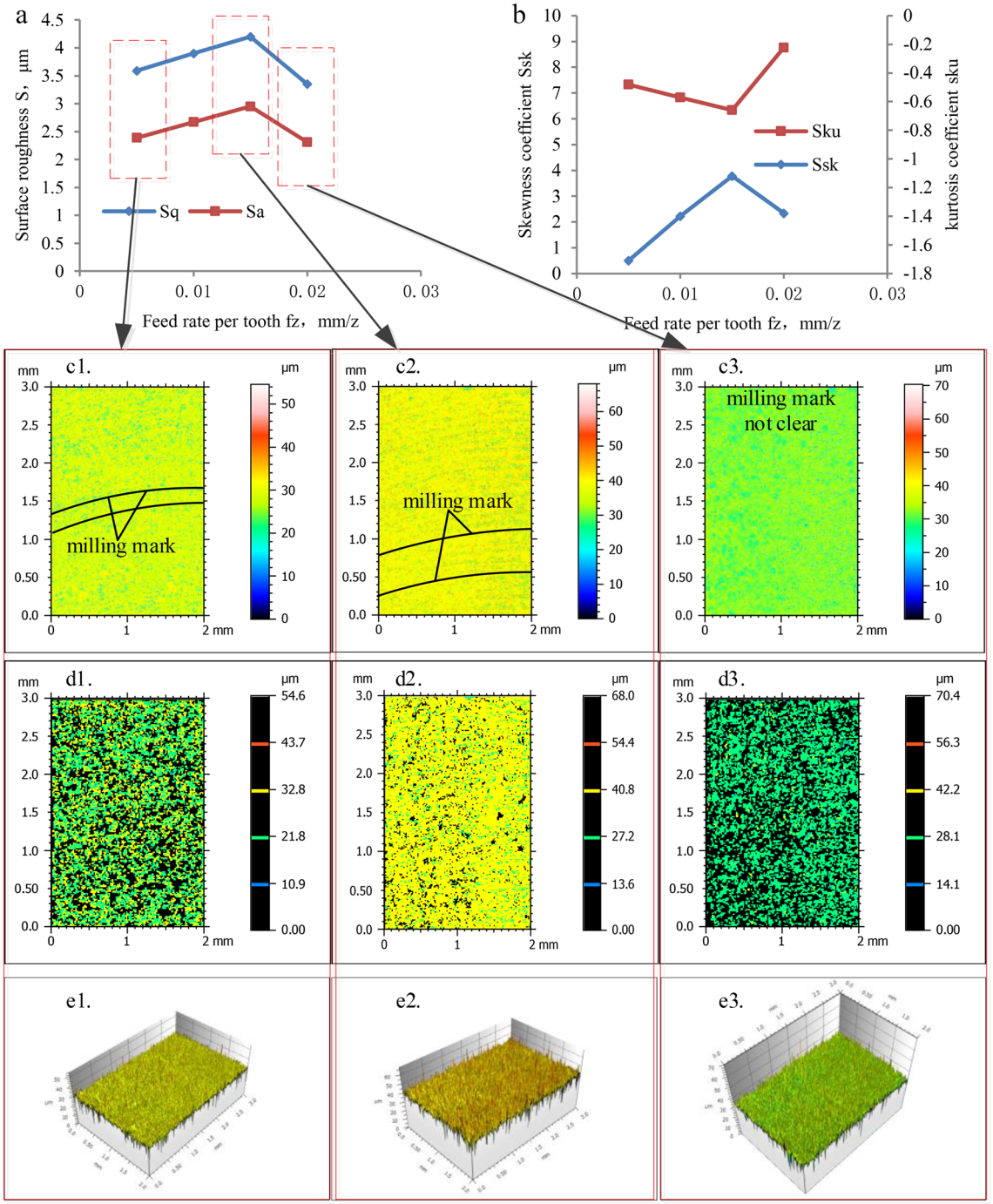

Fig. 12 Surface roughness in variable feed test, $n = 3000$ r/min, $a_p = 0.1$ mm. (a. Surface roughness S_a and S_q; b. Surface skewness coefficient S_{sk} and kurtosis coefficient S_{ku})

propagation is faintly visible, mainly manifested as brittle removal. In the feed rate range of 0.005–0.015 mm/z, there are no cracks on the surface, and this parameters exhibited ductile removal. Among them, the feed rate of 0.015 mm/z (Fig. 12d2) corresponds to fewer pore defects but higher roughness compared to the feed rate of 0.005 mm/z (Fig. 12d1), which is mainly caused by the height of the milling mark contour. From the three-dimensional contour in Fig. 12e1–e3, the contour height at feed rate of 0.015 mm/z is higher, corresponding to greater roughness, while 0.005 mm/z (Fig. 12e1) and 0.02 mm/z (Fig. 12e3) correspond to ductile removal and brittle removal, respectively, whose machining surface contour height is smaller compared to 0.015 mm/z

Table 6 Comparison of different ways for the determination of brittle-ductile transformation region of SiC ceramics machining

Parameters	Force evidence	Roughness evidence	Micro surface evidence	Chip evidence
Cutting depth, mm	Not obvious	0.15–0.2	$\leq 0.1, \geq 0.2$	0.2
Feed rate, mm/z	0.015–0.02	0.015–0.02	0.015–0.02	Not under 0.15

(Fig. 12e2), and the corresponding roughnesses are also smaller.

4.2 Characteristic analysis of two material removal modes affected by tool wear

4.2.1 Effect of tool wear on material removal mode and its force characteristics

When the same parameters are used, the material removal mode may also change due to different tool states, such as the results of the continuous variable feed test with the same

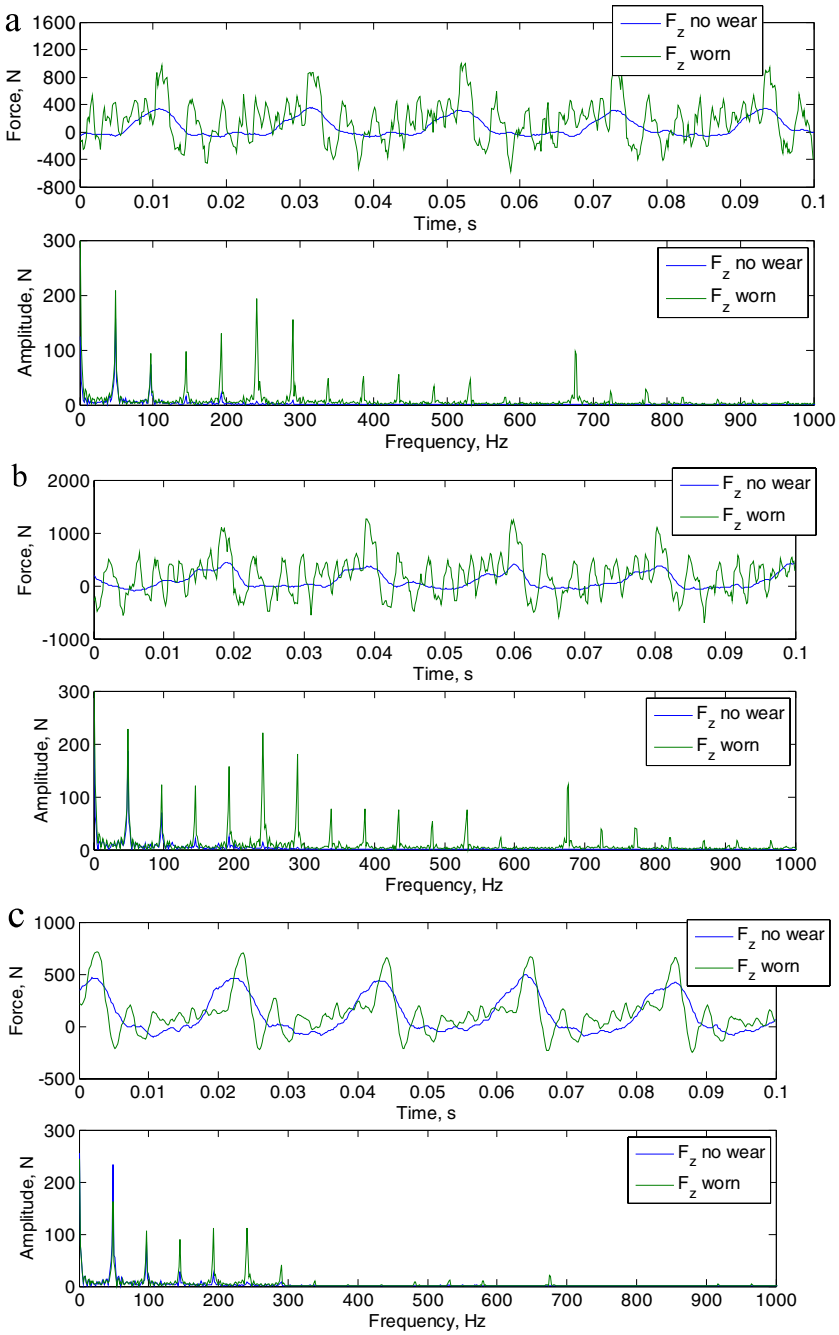

Fig. 13 Force signals before and after tool wear in variable feed rate cutting, $n = 3000$ r/min, $a_p = 0.1$ mm. (a. $f_z = 0.005$ mm/z; b. $f_z = 0.015$ mm/z; c. $f_z = 0.02$ mm/z)

parameters used in the identification test of the cutting force coefficient mentioned above.

Taking the cutting force of Z direction as an example, the variable feed cutting tests with the same cutting parameters are repeated after a series of cutting tests. Because of tool wear, the cutting force increases, and the cutting force signals in the same tooth cycle become disordered with many frequency components, as shown in Fig. 13. Compared with the smooth cutting force signals of no worn tool, more peaks appear, and the most prominent peak value in time domain of worn tool signals becomes steep.

No matter the tool is worn or not, the frequency components of the cutting force signals are the rotation frequency of the tool teeth, but more frequency components appear in the high frequency range of the worn tool signals. In the frequency range of more than 500 Hz, there are almost no frequency components in the no wear signals, while the peak values in the high frequency range of the worn tool signals from feed rate of 0.005 to 0.015 mm/z are still very large, as shown in Fig. 13. When the feed rate increases from 0.015 to 0.02 mm/z, the cutting force is reduced, and the high frequency components in frequency domain disappear, which means the material removal mode changes from ductile removal to brittle removal.

Figure 14 shows the frequency peak comparison of force signals in the two variable feed rate cutting tests with different tool status and the same parameters in frequency domain. The peak values of worn tool in frequency domain are larger than that of unworn tool. A larger feed rate corresponds to a larger amplitude. Both peak values of the first 2 orders frequencies of unworn tool and worn tool in frequency domain are larger. The peak values of worn tool near the 5th harmonic and 14th harmonic are larger.

The peak values of worn tool with feed rate of 0.015 mm/z are greater than that of 0.005 mm/z. The peak frequency at 0.02 mm/z is obviously smaller than that of the other two parameters, and the difference between the first 3 orders is larger. These indicate that the material removal mode has changed. It is found the cutting forces of SiC ceramics depend on the material removal mode. When the material removal modes are different, and even both brittle removal but different proportion of brittle-ductile removal, the cutting forces are different. For force signals in frequency domain with no worn tool in the ductile removal range, the number of frequency components at feed rate of 0.015 mm/z is more than that of 0.005 mm/z. When the feed rate exceeds 0.015 mm/z to 0.02 mm/z, the number of the high frequency components of worn tool reduces.

4.2.2 Tool wear process

Figure 15 shows the wear mechanism of diamond cutting tool for SiC ceramics cutting by analyzing the test data, such as cutting forces, surface roughness, and micrograph. At the beginning of cutting (A), the machining is stable, and the cutting forces signals are like that shows in Fig. 16(a), the tool does not wear (B). With cutting continuously carried on, heat and vibration are produced in the cutting zone, which make one side of the tool teeth crack and collapse (B1), or not broken but worn in a small range (B2). Currently, one tool tooth defects, as a result, unbalance forces signal with periodic

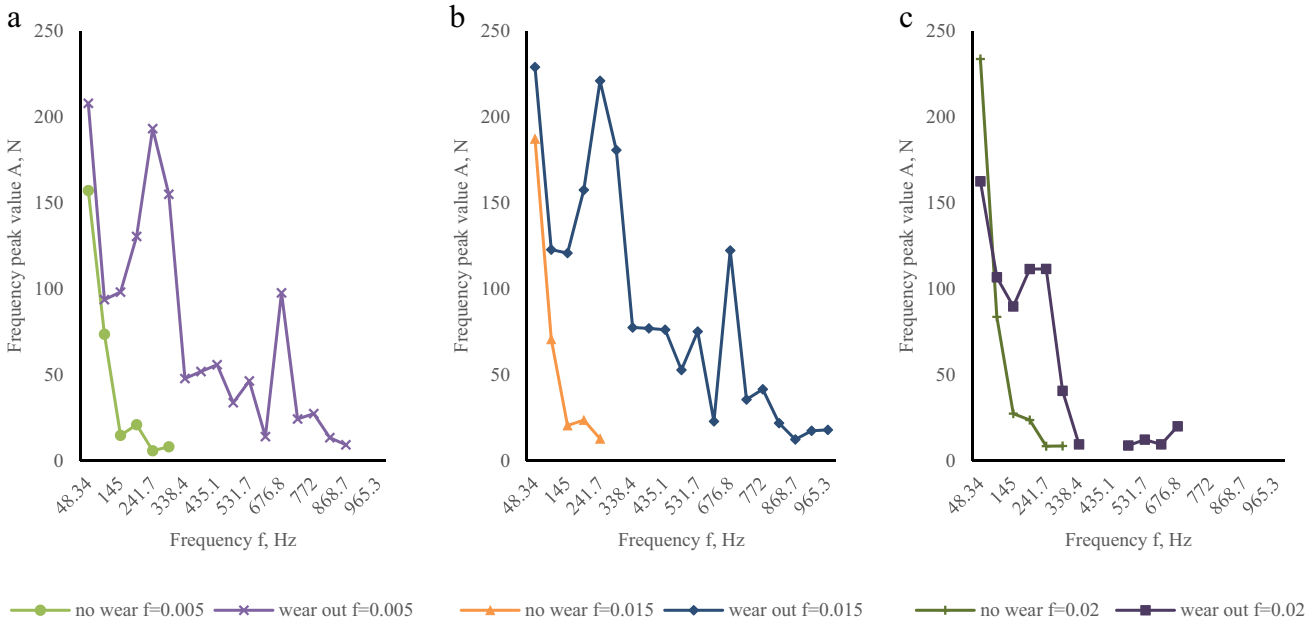

Fig. 14 Force frequency before and after tool wear. (a. $f_z = 0.005$; b. $f_z = 0.015$; c. $f_z = 0.02$)

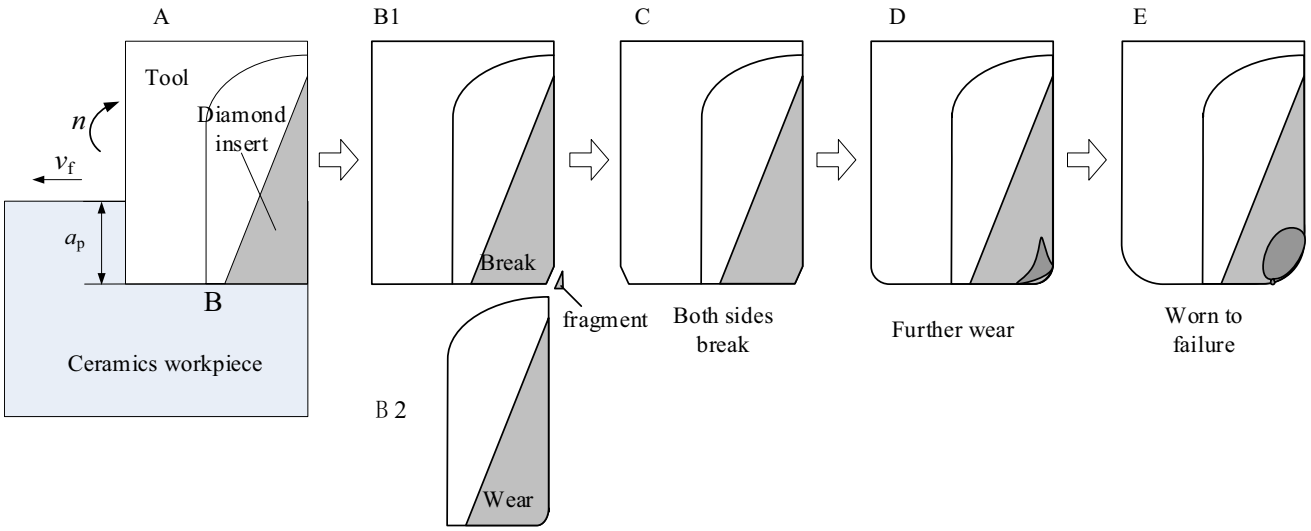

Fig. 15 Wear mechanism of diamond tools in milling SiC ceramics

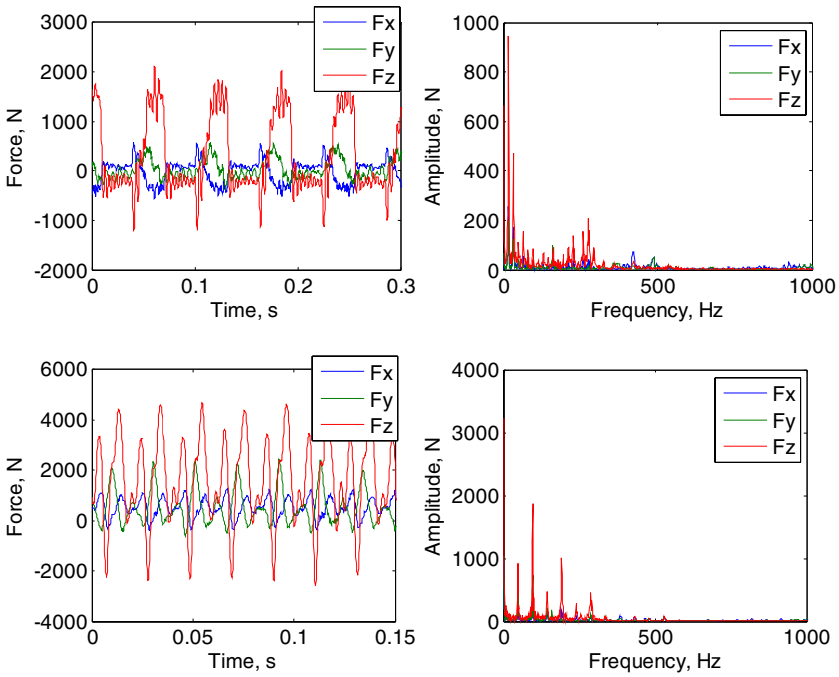

Fig. 16 Comparison of cutting forces for complete and single edge wear. (a. Cutting force when the tool is not worn, $n=3000, f_r=0.005, a_p=0.1$; b. Cutting force of single edge wear, $n=4000, f_r=0.01, a_p=0.2$)

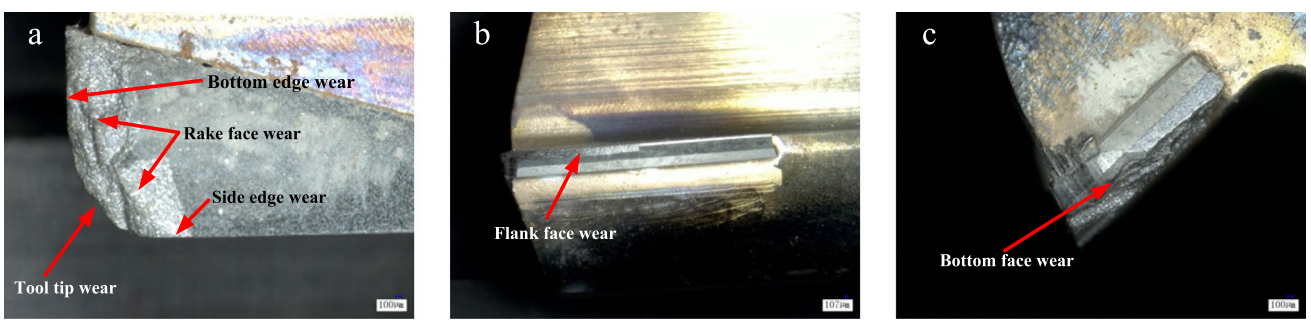

Fig. 17 Tool surfaces, worn tool. (a. rake face 50×; b. flank face 20×; c. bottom face 50×)

fluctuation appear. The cutting performance of tool reduces, as shown in Fig. 16(b).

When the cutting is accumulated to a certain strength, another tool tooth withstands the cutting load begin to break or wear (C). At this point, the processing recover balance with double wear teeth, and the cutting forces signals are symmetrical. Subsequently, the two teeth in the process continuously wear (D). The wear form is rake face collapse in common (Fig. 17a). When the wear reaches a certain distance, the rake face (Fig. 17a), flank face (Fig. 17b) and bottom face (Fig. 17c) of diamond inserts damage with a large wear area. And the cutting tool is worn to failure (E).

Different from metal cutting, diamond tools do not produce crater wear on the rake face when cutting hard and brittle SiC materials, but present gradient chipping and spalling, resulting in the gradual loss of sharpness on the rake face of diamond tools, such as Fig. 17a shows. On the flank wear of tool as shown in Fig. 17b, it is related to the cutting depth on the height of tool and take on gradient spalling similar to that on the rake face, where the cutting capability of tool is gradually weakened from the top to the bottom of the tool. The wear of the tool surface on the bottom of tool decreases gradually from the inner side of the tool to the outer of the tool, as shown in Fig. 17c. From the final wear form of cutting edge, the cutting edge is formed from the right angle in the initial to the arc at the end of tool worn to failure. The tool wear failure can be determined by the increasing of cutting force in the time domain. Also, it can be considered that tool wear tends to failure when the force frequency and amplitude increase significantly. According to the shape of the cutting edge, it can be judged that the wear of the tool tip is in the arc shape, and the delamination of the tool material on the rake face can be comprehensively judged that the tool is approaching failure. At this time, the tool needs to be replaced.

4.2.3 Tool wear and material removal

In each tooth rotation cycle, when tool tooth rotates close to the position of the maximum chip thickness, the material removal mode will change from ductile removal to brittle removal. It can also be considered the material removal will be combined with brittle collapse and ductile removal.

The wear of the two cutting edges at the positions of tool rake face, main cutting edge, secondary cutting edge and tool tip radius increase with the increase of material removal volume, as shown in Fig. 18. A single tooth of the cutting tool will be first worn or damaged, then, the tool rotation is unbalance. When the wear continues, the two teeth are worn or damaged. With the increasing of material removal volume, the cutting edges are worn into arc shape. The cutting of brittle materials is easy to cause cracks. After material removal volume exceeds 3000 mm^3, tool wear increases significantly.

5 Conclusion

In this paper, the influence of parameters and tool wear on brittle-ductile material removal mode during SiC ceramic milling were studied. Some conclusion can be summaried as follows:

(1) The models of critical load of brittle material fracture and the chip thickness of ceramics cutting are used to descript the stability interval of brittle-ductile transition. Results were found that the fracture of brittle material is the cause of brittle removal. As the stress does not reach the fracture strength, the material is ductile removal. When the stress exceeds the critical strength, brittle removal occurs. Evidence of chip mor-

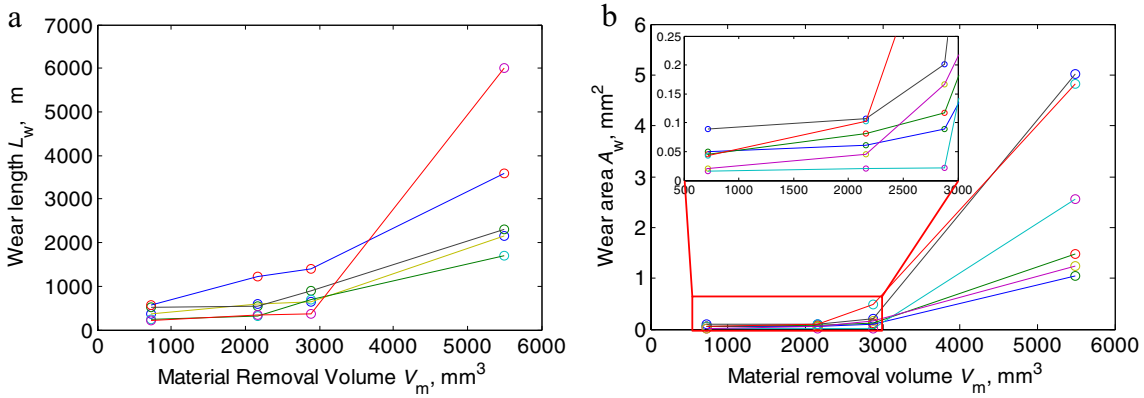

Fig. 18 Tool wear length and wear area with material removal volume. (a. relationship between tool wear length and MRR; b. relationship between tool wear area and MRR)

phology and surface roughness were present to prove the material removal mode has changed. Powder chip was found in ductile removal process, while block chips generate in the brittle removal process. Better surface integrity can be controlled in the ductile cutting, while surface defects can be found on the brittle removal surfaces.

(2) The change in material removal mode is due to the changes of cutting parameters. Excessive cutting parameters are the factor that triggers the change in material removal mode. When the parameters exceed the critical parameters for mode change, material removal will transition from ductile removal to brittle removal. The cutting is controlled in a ductile removal mode if the undeformed chip thickness does not exceed the critical size of the ceramics fracture. Generally, material removal is accompanied by brittle and ductile modes, brittle–ductile transition is mainly determined by the proportion of the two removal modes.The proportion of the brittle failure of ceramics milling can be reduced with the decreasing of feed rate and cutting depth. The critical parameter interval of feed rate in SiC ceramics milling is 0.015–0.02 mm/z, while the critical cutting depth is 0.15–0.2 mm.

(3) Tool wear is another factor that affects the transition of brittle-ductile removal mode in milling SiC ceramics. When the tool is not worn, multiple cutting tests with the same parameters can prove that the distribution of cutting force is linearly monotonic and the data repeatability is consistent. After the tool is worn, the cutting force significantly increases compared to the cutting force with the same parameters when the tool is not worn, making it more prone to brittle removal. The frequency of cutting force with worn tool reduces the high-frequency component compared to the ductile removal frequency when the tool is not worn, which is one of the evidence to prove that the brittle removal mode becomes the main material removal mode after tool wear. With the increasing of cutting volume, the tool edges are worn into arc shape. The wear area increases sharply when material removal volume exceeds 3000 mm^3.

(4) The milling force coefficient of SiC was also studied. Under the ductile removal conditions, the force coefficient can be identified according to the linear distribution of cutting force. When the material removal transitions to brittle removal, the cutting force mixed with brittle removal and ductile removal is not suitable for identifying the cutting force coefficient.

Acknowledgements This work is supported by Key Research and Development Program of Shandong Province, China (No. 2022CXGC010201), National-Local Joint Engineering Laboratory of NC Machining Equipment and Technology of High-Grade stone SJSC-2015-11, China. The authors would like to express their appreciation to the agencies.

Declarations

Conflict of interest The authors declare no competing interests.

References

1. Wenbo Z, Honghua S, Jianbo D, Tengfei Y, Yihao Z (2018) Numerical investigation on the influence of cutting-edge radius and grinding wheel speed on chip formation in sic grinding. Ceram Int 44:21451–21460
2. Zhang K, Su H, Xu W (2014) Influence of plate wheel dressing of monolayer brazed diamond wheel on material removal mechanism in SiC grinding, Journal of Nanjing University of Aeronautics and Astronautics 46(5):732–737
3. Li Z, Zhang F, Luo X, Chang W, Cai Y, Zhong W (2019) Material removal mechanism of laser-assisted grinding of rb-sic ceramics and process optimization. J Eur Ceram Soc 39:705–717
4. Chang CW, Kuo CP (2007) An investigation of laser-assisted machining of Al2O3 ceramics planning. Int J Mach Tool Manu 47(3–4):452–461
5. Zhang S, Qi YZ, Chen JY (2023) Brittle-ductile transition behavior of 6H-SiC in oblique diamond cutting. Int J Mech Sci 246:108155
6. Sun ZW, To S (2023) Ductile Machining Mechanism for Microstructure by Ultra-precision Raster Milling. In: To S, Wang S (ed) Fly Cutting Technology for Ultra-precision Machining. Springer, Singapore, pp 305–326
7. Cao J, Nie M, Liu Y (2018) Ductile-brittle transition behavior in the ultrasonic vibration-assisted internal grinding of silicon carbide ceramics. Int J Adv Manuf Tech 96:9–12
8. Zhang Y, Li C, Ji H, Yang X, Yang M, Jia D, Zhang X, Li R, Wang J (2017) Analysis of grinding mechanics and improved predictive force model based on material-removal and plastic-stacking mechanisms. Int J Mach Tools Manuf 122:81–97
9. Zhao L, Zhang JJ, Zhang JG, Hartmaier A (2020) Atomistic investigation of machinability of monocrystalline 3c-sic in elliptical vibration-assisted diamond cutting. Ceram Int 47:2358–2366
10. Yang M, Li C, Zhang Y, Jia D, Li R, Hou Y, Cao H (2019) Effect of friction coefficient on chip thickness models in ductile-regime grinding of zirconia ceramics. Int J Adv Manuf Tech 102:2617–2632
11. Chen ST, Yang KC (2022) Semi-ductile cutting regime technology for machining Zerodur glass-ceramic microstructures. Precis Eng 74:92–109
12. Priyadarshini M, Pradhan S, Samantray R (2023) Methods for ceramic machining. in: Gupta R K, Behera A, Farhad S (ed) Advanced Flexible Ceramics. Elsevier, Amsterdam, pp 243–257
13. Demarbaix A, Ducobu F, Juste E, Petit F, Duterte C, Lorphèvre ER (2021) Experimental investigation on green ceramic machining with nanosecond laser source. J Manuf Process 61:245–253

14. Fan MX, Zhou XQ, Song JZ (2024) Experimental investigation on cutting force and machining parameters optimization in in-situ laser-assisted machining of glass–ceramic. Opt Laser Technol 169:110109
15. Rao X, Zhang F, Liu L (2016) Surface characteristics for RB-SiC ceramics by electrical discharge diamond grinding. Opt Precis Eng 24(9):2192–2199
16. Liu YH, Ji RJ, Li Q, Yu L, Li X (2009) An experimental investigation for electric discharge milling of sic ceramics with high electrical resistivity. J Alloy Compd 472(1–2):406–410
17. Guo YF, Feng YR, Wang L (2018) Experimental investigation of EDM parameters for zrb2-sic ceramics machining. Procedia CIRP 68:46–51
18. Mohri N, Fukuzawa Y, Tani T, Saito N, Furutani K (1996) Assisting electrode method for machining insulating ceramics. CIRP Ann-Manuf Techn 45(1):201–204
19. Sánchez JA, Cabanes I, Lacalle LNLD, Lamikiz A (2001) Development of optimum electrodischarge machining technology for advanced ceramics. Int J Adv Manuf Tech 18(12):897–905
20. Goel S, Luo X, Comley P, Reuben RL, Cox A (2013) Brittle–ductile transition during diamond turning of single crystal silicon carbide. Int J Mach Tool Manu 65(2):15–21
21. Liang Z, Wang X, Wu Y (2013) Experimental study on brittle - ductile transition in elliptical ultrasonic assisted grinding (euag) of monocrystal sapphire using single diamond abrasive grain. Int J Mach Tool Manu 71(8):41–51
22. Wang B, Liu Z, Su G (2015) Investigations of critical cutting speed and ductile-to-brittle transition mechanism for workpiece material in ultra-high speed machining. Int J Mech Sci 104:44–59
23. Beaucamp A, Simon P, Charlton P, King C, Matsubara A, Wegener K (2017) Brittle-ductile transition in shape adaptive grinding (SAG) of SiC aspheric optics. Int J Mach Tool Manu 115:29–37
24. Xiao G, To S, Zhang G (2015) Molecular dynamics modelling of brittle–ductile cutting mode transition: Case study on silicon carbide. Int J Mach Tool Manu 88:214–222
25. Marshall DB, Lawn BR (1985) Indentation of brittle materials, micro indentation technology in materials science and engineering. International Metallographic Society 1:889
26. Shamray S, Azarhoushang B, Paknejad M, Buechler A (2022) Ductile-brittle transition mechanisms in micro-grinding of silicon nitride. Ceram Int 48(23):34987–34998
27. Malkin S (1989) Grinding technology: theory and applications of machining with abrasives, Wiley, New York
28. Arif M, Rahman M, San WY (2012) Analytical model to determine the critical conditions for the modes of material removal in the milling process of brittle material. J Mater Process Tech 212(9):1925–1933
29. Jacob J (2014) Determination of the ductile to brittle transition and critical depth of cut in 6H-silicon carbide through fly cutting. https://www.researchgate.net/publication/237675955_DETERMINATION_OF_THE_DUCTILE_TO_BRITTLE_TRANSITION_AND_CRITICAL_DEPTH_OF_CUT_IN_6H-SILICON_CARBIDE_THROUGH_FLY_CUTTING
30. Scattergood O, Blake N (1990) Ductile-regime machining of germanium and silicon. J Am Ceram Soc 73(4):949–957
31. Hiroaki T, Shoichi S (2013) Damage-free machining of monocrystalline silicon carbide. CIRP Ann-Manuf Techn 62(1):55–58
32. Qiao Y, Argon AS (2003) Brittle-to-ductile fracture transition in fe–3wt.%si single crystals by thermal crack arrest. Mech Mater 35(9):903–912
33. Toshihiko H, Tomokazu K, Atsushi H (2012) Surface roughness control based on digital copy milling concept to achieve autonomous milling operation. Procedia CIRP 4(4):35–40
34. Zhou M, Wang XJ, Ngoi BKA, Gan JGK (2002) Brittle - ductile transition in the diamond cutting of glasses with the aid of ultrasonic vibration. J Mater Process Tech 121(2–3):243–251
35. Campbell GH, Dalgleish BJ, Evans AG (2010) Brittle-to-ductile transition in silicon carbide. J Am Ceram Soc 72(8):1402–1408